

Molecular Subtypes of Clear Cell Renal Cell Carcinoma Are Associated with Sunitinib Response in the Metastatic Setting

Benoit Beuselinck^{1,2,3,5}, Sylvie Job⁶, Etienne Becht^{2,3,4}, Alexandra Karadimou^{1,2,3}, Virginie Verkarre^{2,7}, Gabrielle Couchy^{1,2,3}, Nicolas Giraldo^{2,4}, Nathalie Rioux-Leclercq⁸, Vincent Molinié⁹, Mathilde Sibony^{2,10}, Reza Elaidi⁵, Corinne Teghom⁵, Jean-Jacques Patard¹¹, Arnaud Méjean^{2,5}, Wolf Herman Fridman^{2,3,4}, Catherine Sautès-Fridman^{2,3,4}, Aurélien de Reyniès⁶, Stéphane Oudard^{2,5}, and Jessica Zucman-Rossi^{1,2,3,5}

Abstract

Purpose: Selecting patients with metastatic clear-cell renal cell carcinoma (m-ccRCC) who might benefit from treatment with targeted tyrosine kinase inhibitors (TKI) is a challenge. Our aim was to identify molecular markers associated with outcome in patients with m-ccRCC treated with sunitinib.

Experimental Design: We performed global transcriptome analyses on 53 primary resected ccRCC tumors from patients who developed metastatic disease and were treated with first-line sunitinib. We also determined chromosome copy-number aberrations, methylation status, and gene mutations in *von Hippel-Lindau* and *PBRM1*. Molecular data were analyzed in relation with response rate (RR), progression-free survival (PFS), and overall survival (OS). Validation was performed in 47 additional ccRCC samples treated in first-line metastatic setting with sunitinib.

Results: Unsupervised transcriptome analysis identified 4 robust ccRCC subtypes (ccrcc1 to 4) related to previous molecular classifications that were associated with different responses

to sunitinib treatment. ccrcc1/ccrcc4 tumors had a lower RR ($P = 0.005$) and a shorter PFS and OS than ccrcc2/ccrcc3 tumors ($P = 0.001$ and 0.0003 , respectively). These subtypes were the only significant covariate in the multivariate Cox model for PFS and OS ($P = 0.017$ and 0.006 , respectively). ccrcc1/ccrcc4 tumors were characterized by a stem-cell polycomb signature and CpG hypermethylation, whereas ccrcc3 tumors, sensitive to sunitinib, did not exhibit cellular response to hypoxia. Moreover, ccrcc4 tumors exhibited sarcomatoid differentiation with a strong inflammatory, Th1-oriented but suppressive immune microenvironment, with high expression of *PDCD1* (*PD-1*) and its ligands.

Conclusions: ccRCC molecular subtypes are predictive of sunitinib response in metastatic patients, and could be used for personalized mRCC treatment with TKIs, demethylating or immunomodulatory drugs. *Clin Cancer Res*; 21(6): 1329–39. ©2015 AACR.

¹Inserm, UMR-1162, Génomique fonctionnelle des tumeurs solides, Paris, France. ²Université Paris Descartes, Sorbonne Paris Cité, Faculté de Médecine, Paris, France. ³Labex Immuno-oncology, Paris, France. ⁴UMR_S1138, Centre de Recherche des Cordeliers, Paris, France. ⁵Assistance Publique-Hôpitaux de Paris, Hôpital Européen Georges Pompidou, Department of Oncology, Paris, France. ⁶Programme Cartes d'Identité des Tumeurs, Ligue Nationale Contre le Cancer, Paris, France. ⁷Assistance Publique-Hôpitaux de Paris, Hôpital Necker-Enfants malades, Department of Pathology, Paris, France. ⁸Department of Pathology, CHU Rennes, Rennes, France. ⁹Department of Pathology, Clinique St-Joseph, Paris, France. ¹⁰Assistance Publique-Hôpitaux de Paris, Hôpital Cochin, Department of Pathology, Paris, France. ¹¹Department of Urology, Hôpital Bicêtre, Le Kremlin-Bicêtre, France.

Note: Supplementary data for this article are available at Clinical Cancer Research Online (<http://clincancerres.aacrjournals.org/>).

B. Beuselinck and S. Job contributed equally to this article.

A. de Reyniès and S. Oudard contributed equally to this article.

Corresponding Author: Jessica Zucman-Rossi, Inserm UMR-1162, Génomique fonctionnelle des tumeurs solides, 27 rue Juliette Dodu, F-75010 Paris, France. Phone: 33-1-53725166; Fax: 33-1-53725192; E-mail: jessica.zucman-rossi@inserm.fr

doi: 10.1158/1078-0432.CCR-14-1128

©2015 American Association for Cancer Research.

Introduction

Targeted therapies (TT) have significantly improved the prognosis of patients with metastatic clear-cell renal cell carcinoma (m-ccRCC). Sunitinib is a tyrosine kinase inhibitor (TKI) targeting *VEGFR* that significantly prolongs progression-free survival (PFS), but not overall survival (OS), as compared with IFN α (1, 2). Currently, it is an approved first-line treatment option for patients with m-ccRCC. However, in the pivotal phase III trial, 7% of patients experience progressive disease (PD) upon RECIST at their first evaluation, and virtually all patients ultimately develop PD (2). In routine clinical practice, primary PD rate is higher and may reach 20%. Although several prognostic factors of survival in patients with m-ccRCC receiving TT have been described and several resistance mechanisms have been proposed (3), no reliable biomarkers of sunitinib sensitivity or primary/secondary resistance have been identified.

Recent unsupervised gene expression analysis of 48 ccRCCs identified two molecular ccRCC subtypes (*ccA* and *ccB*; ref. 4). A meta-analysis of 480 ccRCCs confirmed this classification and identified a third subtype, *cluster_3*, associated with a wild-type von Hippel-Lindau (VHL) gene profile (5). The Cancer Genome Atlas (TCGA) project subsequently highlighted four ccRCC

Translational Relevance

After 10 years of routine clinical use of tyrosine kinase inhibitors (TKI) in metastatic clear-cell renal cell carcinoma (m-ccRCC), the selection of patients who might benefit from this treatment remains a challenge. In this translational work, based on a large series of fresh-frozen kidney tumor samples combined with an extended clinical database, we have defined four robust molecular subtypes of m-ccRCC significantly associated with different responses to sunitinib. This work not only provides the first integrative genomic study of m-ccRCC but it also identifies subtypes of tumors resistant to sunitinib and associated with poor survival. These molecular subtypes of tumors are characterized by a stem-cell polycomb signature, a CpG hypermethylation, sarcomatoid differentiation, and a strong inflammatory, Th1-oriented but suppressive immune microenvironment. These new molecular signatures could be used for a more personalized m-ccRCC treatment to administer TKIs, demethylating or immunomodulatory drugs, according to the molecular typing of the tumors.

subtypes (6). In both studies, postnephrectomy survival was related to ccRCC subtype. A poor prognosis was also associated with somatic mutations in *BAP1* and *SETD2* (7, 8) and with chromosome amplifications or losses at 8q, 14q, or 9p (9–12). However, no associations have been made between molecular features and outcome in patients with m-ccRCC on TT (13).

We hypothesized that an integrated genomic analysis of primary ccRCCs might help to identify subgroups of ccRCCs more sensitive or resistant to anti-VEGFR TT. Thus, the aim of our study was to determine whether expression profiles, genomic abnormalities, mutational status, and epigenetic changes were related to outcomes after first-line sunitinib in patients with m-ccRCC.

Materials and Methods

Included patients

Primary ccRCC specimens were collected from 121 patients undergoing nephrectomy in 19 French and one Belgian hospitals from 1994 to 2011 (patient characteristics in Supplementary Table S1). For inclusion in the study, patients had to have developed synchronous or metachronic metastases, received sunitinib (50 mg/day, 4 weeks on/2 weeks off) as first-line treatment in the metastatic setting (prior cytokine therapy was allowed), completed at least one 28-day cycle of sunitinib, and undergone their first CT scan assessment.

Drug schedule and dose-reduction policy complied with local practice guidelines. Follow-up chest/abdomen CT scans were performed every 2 cycles of treatment. Study endpoints were response rate (RR) according to RECIST 1.0, PFS, and OS. Four expert genitourinary pathologists blinded to patient outcome reviewed all nephrectomy pathology slides. The protocol was approved by the medical ethics review boards of all participating institutions. Signed consent was obtained from all patients in accordance with French and Belgian legislations. Frozen biologic material from deceased patients was used when prior agreement for such use had been given by the institutional review board.

Datasets and preprocessing

Dataset for transcriptome (E-MTAB-3267), SNP (E-MTAB-3269) and methylome (E-MTAB-3274) are available at ArrayExpress (<https://www.ebi.ac.uk/arrayexpress/>).

Transcriptome data. Transcriptomic profiling was performed using HuGene 1.0ST Affymetrix array for 53 ccRCC samples and 6 adjacent normal tissue samples (NT). Biotinylated single-strand cDNA targets were prepared with 200 ng of total RNA, using the Ambion WT Expression Kit and the GeneChip WT Terminal Labeling Kit according to Affymetrix recommendations.

Methylome data. Whole-genome DNA methylation was analyzed in 102 ccRCCs and 5 adjacent NTs using the Illumina Infinium HumanMethylation450 assay that examines the DNA methylation status of 485,000 CpG sites (covering 99% of RefSeq genes and 96% of CpG islands). Genomic DNA was extracted using either the Manual-MagNa Pure LC DNA II Kit (Roche) or the Manual-Gentra Puregene Kit (Qiagen) and bisulfite-converted using the EZ-96 DNA Methylation Kit (Zymo Research) by IntegraGen SA (<http://www.integragen.com>) and processed according to the Illumina protocol.

Genome data. For chromosome gain/loss profiling, 103 ccRCCs and 5 adjacent NTs were analyzed with Illumina OmniExpress chips, containing 731,442 probes. Hybridization was performed by IntegraGen, according to the manufacturer's instructions. The absolute copy numbers and genotype status of segments were determined using the genome alteration print (GAP) method (14). Segments with an absolute copy number above (respectively below) the ploidy of the sample were considered as gains (respectively losses). The Genomic Identification of Significant Targets In Cancer (GISTIC) methodology (15) was used to identify significantly recurrent chromosome aberrations.

Quantitative RT-PCR. qRT-PCR reactions were performed on 98 ccRCCs and 5 NTs with low density array (LDA) for 65 genes and individual probes for 5 genes as previously described (16). Genes were selected from the differential analysis of the Affymetrix data (ANOVA *q*-value less than 0.05 and an absolute fold change greater than 1.5). Primers and probes for all genes were obtained from Applied Biosystems Taqman Gene Expression Assays. Supplementary Table S2 provides the gene symbol, gene name, and Applied Biosystems Assay ID number for the genes studied.

For details on overlap between samples used for each omics, see Supplementary Table S3.

Mutation analysis

Tumors were screened for *VHL* and *PBRM1* mutations (Supplementary Table S4) using direct sequencing (primers and protocols available on request).

Omics analysis

Unsupervised classification. For unsupervised class discovery within the four omics, three methods were used: the recursively partitioned mixture model (RPMM; ref. 17) and two consensus clustering methods (18, 19). Only the results obtained with the third method were described in the article. Nevertheless, we showed a strong association between the three methods (Fisher exact *P* values from 3.9e–19 to 2.92e–21). We used the gap statistic to determine the number of clusters (20).

Differential analysis. We used moderate *T* tests to identify genes differentially expressed between groups of samples, using limma R-package. ANOVA models were used for multigroup comparison. To control for multiple testing, we measured the local FDR using the Benjamini and Hochberg method (R-package stats).

Association analysis. We evaluated the association between unsupervised or supervised subgroups and the bioclinical factors using χ^2 or Fisher exact test. For each clinical characterization, all covariates were analyzed but only the significant covariates were shown ($P \leq 0.05$). The bioclinical factors included tumor–node–metastasis, Eastern Cooperative Oncology Group Performance Status (ECOG-PS), International Metastatic Renal Cell Carcinoma Database Consortium (IMDC), Fuhrman, or Memorial Sloan Kettering Cancer Center (MSKCC) scores, systemic treatment, hemoglobin (<11.5 g/dL in women, <13.0 g/dL in men), platelets (>400,000/mm³), lactate dehydrogenase (>1.5× upper limit of normal), neutrophils (>4,500/mm³), calcium (>10 mg/dL), pathologic characteristics such as eosinophils, necrosis, or inflammation, rhabdoid, and sarcomatoid phenotypes.

Fisher exact or χ^2 tests were used to select the recurrent chromosome aberrations identified by GISTIC that are differential between groups. Criteria of sensitivity and specificity were added to select aberrations characteristic of a given subgroup. An aberration was characteristic of a given subgroup if the sensitivity and the specificity are >0.65.

Signaling pathway analysis. To identify biologic features associated with ccRCC molecular subtypes, 17,306 pathways collected from KEGG, GO, MSigDB, SMD, and Biocarta (and related genes) were tested. A hypergeometric test was used to measure the association between a gene (probe set) list—related to a given molecular subtype (see below)—and a biologic pathway or a gene ontology term (GO term), as in GOstats R-package from R. Gentleman. Pathway analyses were performed on transcriptome data, methylome data, and methylome data anticorrelated with transcriptome data (correlation test $P \leq 0.05$ and correlation coefficient <0). In this pathways analysis, the gene lists related to each molecular subtypes corresponded to (i) genes specifically upregulated in the subtype (respectively hypermethylated), (ii) genes specifically downregulated in the subtype (respectively hypomethylated), and (iii) genes both up and downregulated (respectively hyper- and hypomethylated) in the subtype.

Survival analysis. Survival time was calculated from the first sunitinib treatment. Patients who were lost to follow-up or alive at the time of the study were treated as censored events. Survival curves were calculated according to the Kaplan–Meier method (function Surv, R-package survival, V2.29), and differences between curves were assessed using the log-rank test (function survdiff, R-package survival).

To find clinical criteria related to PFS or OS, univariate models were performed on all the pathologic and clinical covariates (function coxph, R-package survival). Covariates showing a significant association to prognosis (log-rank $P < 0.05$) at the univariate level were selected to be analyzed in multivariate models, after the exclusion of redundant covariates (ex MSKCC- and IMDC scores).

Classifier building. The training set was composed of 51 samples with Affymetrix and qRT-PCR, and the validation set was composed of 47 samples with only qRT-PCR.

A first centroid-based predictor was built to assign a sample to one of the three following groups ccrcc1&4/ccrcc2/ccrcc3 using a subset of the differentially expressed genes between these three groups. A gene was defined differentially expressed in a subtype when the ANOVA *P* value was <0.05 and when the absolute fold change with the other subtypes was >0.5. The optimal subset of 27 genes was obtained by a step-by-step strategy by optimizing the success rate. The DLDA-dissimilarity measure was then used to predict the subtype (Supplementary Table S2).

For samples predicted as ccrcc1&4 (using the predictor mentioned above), a second centroid-based predictor was built to assign each sample to one of the two subtypes ccrcc1 or ccrcc4. A subset of the differentially expressed genes between ccrcc1 and ccrcc4 subtypes was used. A gene was defined differentially expressed between the two subtypes when the ANOVA *P* value was <0.05 and when the absolute fold change was >3. The optimal subset of 8 genes was obtained by a step-by-step strategy by optimizing the success rate. The DLDA-dissimilarity measure was then used to predict the subtype.

The obtained centroid-based predictors were applied on two public datasets: The Brannon expression dataset (GEO-website, GSE33093; ref. 5) and TCGA dataset (6).

Use of immune metagenes

The datasets mentioned by Bindea and colleagues (21) were downloaded and normalized separately using the fRMA Bioconductor package. Cancer cell lines dataset GSE5720 was also retrieved from Gene Expression Omnibus and normalized using fRMA. Samples GSM133550, GSM133594, GSM133638, GSM133657, which correspond respectively to ccRCC cell lines ACHN, SN12C, UO-31, and Caki-1, were added. All probesets identified included in the five metagenes used in our work (NK CD56dim, Cytotoxic cells, T cells, B cells, macrophages) were checked for expression by kidney cancer cell lines. One hundred thirty-eight of 142 probesets were completely specific and sensitive to predict immune cell–type against ccRCC cell lines samples, and 134 of 142 probesets had a right-tailed *t* test *P* value < 0.05 when compared with ccRCC cell lines samples. To compute average metagene values in our dataset, log₂ expression values for each probesets were first mapped to gene symbols using average expression of all the corresponding probesets, then this value was centered, and scaled across our dataset. Finally, the mean of all the scaled expressions was taken to represent the signature.

Immunohistochemistry

Formalin-fixed and paraffin-embedded tissue sections (5 μ m) were stained with an anti-CD8 (5.0 μ g/mL; clone SP16; Spring-bioscience) with an autostainer Link 48 (Dako) as previously described (22). Deparaffinization, rehydration, and epitope retrieval were performed in a PT-Link (Dako) in a high pH solution as described by the manufacturer. Tissue sections were first incubated with anti-CD8 (SP16; Springbioscience) and posteriorly with a biotin–streptavidin-coupled antibody. Revelation was done with 3-amino-9-ethylcarbazole substrate (Vector Laboratories).

Results

Patient characteristics and clinical predictors of sunitinib response

In our series of 121 patients, after a median follow-up of 55 months (range, 1.5–86), median PFS and OS were 13 and 27

months, respectively. Forty-seven percent of patients experienced a complete or partial response (CR/PR), 36% stable disease (SD), and 17% early PD following RECIST 1.0. By comparing patients with extreme phenotype (CR/PR vs. PD), we identified several clinical and biologic features associated with a poor sunitinib response: baseline neutrophilia, thrombocytosis, anemia, sarcomatoid differentiation, synchronous metastases at initial diagnosis, poorer ECOG-PS, Heng (23), and MSKCC scores (24, 25; Fig. 1A and B). However, in the overall series of patients, using all the clinical, pathologic, and molecular features and a variety of predictive algorithms (PAM, DLDA, DQDA), supervised analyses failed to identify robust factors predictive of sunitinib response (Supplementary Table S5). As this result could be due to the molecular diversity of the tumors, we investigated the relationships between ccRCC molecular subtypes and response to sunitinib.

Molecular subtypes and sunitinib response

Using the expression profiles of the 1% most variable probe sets ($n = 324$ representing 294 different genes) among the whole series of tissues (53 ccRCCs, 6 NTs), we performed an unsupervised consensus clustering analysis of our series. We identified four robust subgroups of tumors, called ccrc1 to ccrc4 (Fig. 2). In particular, ccrc3 tumors included all NTs and showed a transcriptomic signature closed to normal samples (Fig. 2B and C).

To extend the molecular subtyping to a larger series, we built a qRT-PCR 35-gene classifier (Supplementary Table S6), which correctly classified 94% of the samples from the initial series in ccrc1–4, and was used to predict 47 additional ccRCC tumors.

In the series of 98 patients, nonresponders were enriched in ccrc1 (PD 22%) and ccrc4 (27%) versus 3% and 0% in ccrc2 and ccrc3, respectively (Fig. 3A; Supplementary Table S7). In contrast, responders were over-represented in ccrc2 (PR/CR, 53%) and ccrc3 (70%) compared with 41% and 21% in ccrc1 and ccrc4, respectively ($P = 0.005$; Fig. 3A; Supplementary Table S7). Moreover, ccrc1 and ccrc4 tumors showed a poorer PFS (13, 8, 19, and 24 months, respectively; $P = 0.0003$) and OS (24, 14, 35, and 50 months, respectively; $P = 0.001$) compared with ccrc2 and ccrc3 tumors (Fig. 3B; Table 1; Supplementary Table S7).

Classification of the tumors recoded in ccrc1&4 versus ccrc2&3 was the most significant covariate in univariate Cox analysis with a poorer PFS ($P = 0.004$) and OS ($P = 0.0002$). For the multivariate analysis, in a first step, among all the factors that were associated with PFS and OS in univariate analysis, we excluded those factors that could be overlapping (Table 1). Finally, the following factors were included in the multivariate analysis, both for PFS and OS: IMDC score, the presence of bone metastases, the presence of sarcomatoid dedifferentiation, 8q amplification, and the classification recoded as ccrc2+3 versus ccrc1+4. It remained the only significant covariate in the multivariate Cox model for PFS ($P = 0.017$). In the multivariate Cox model for OS, the recoded classification ($P = 0.0064$) and the presence of bone metastasis ($P = 0.049$) remained as significant covariates (Fig. 3C).

Characterization of the m-ccRCC molecular subtypes

To better understand how each molecular subtype could influence response to sunitinib, we characterized our cohort for somatic mutations in *PBRM1* and *VHL* genes ($n = 117$ tumors), methylation profiling exploring 485,000 nucleotide sites ($n = 102$), and copy number targeting 731,442 genomic loci ($n = 103$). Transcriptome and methylome profiles of the four subtypes were compared using pathway analysis methods, and recurrent copy number aberrations were delimited from the SNP profiles.

The ccrc4 subtype demonstrated specific features at the pathologic level with frequent sarcomatoid differentiation and inflammation (Fig. 4A; Table 2). Accordingly, pathway analysis of transcriptome profiles identified an overexpression of genes related to immune response, chemotaxis, and apoptosis (Fig. 4B). These pathways were also deregulated at the methylome level with hypomethylation of overexpressed genes which could be related to the inflammatory and immune microenvironments characterizing these tumors (Fig. 4C and Supplementary Table S8). The ccrc4 subtype had a high expression of markers of inflammation, such as members of the *TNF* and *IRF* families. The analysis of cytokines revealed a strong expression of myeloid and T cells homing factors and their corresponding receptors and Th-1-related factors such as $IFN\gamma$ and IL12. The immune suppressive

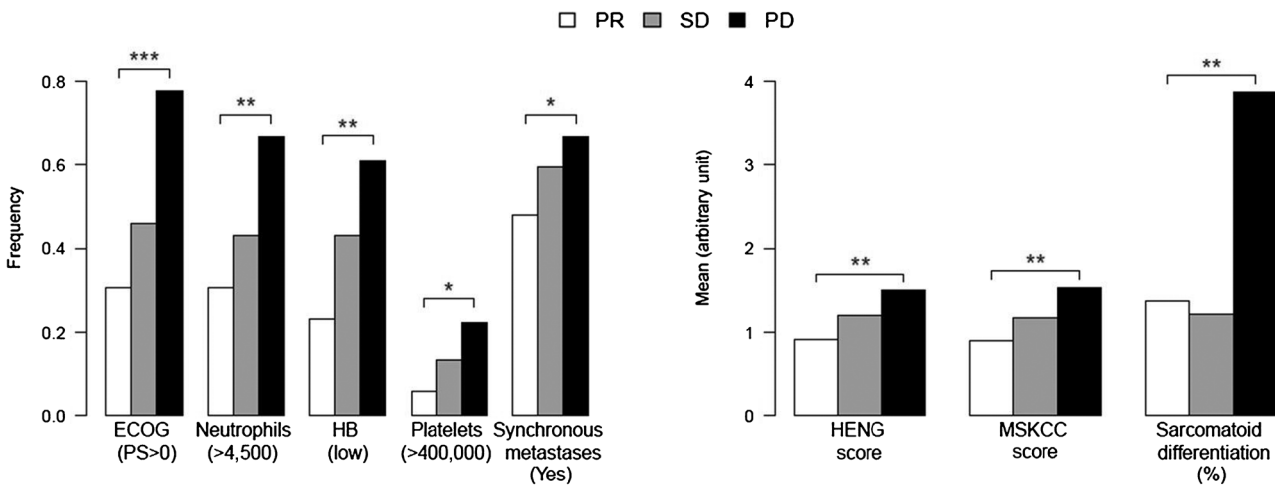
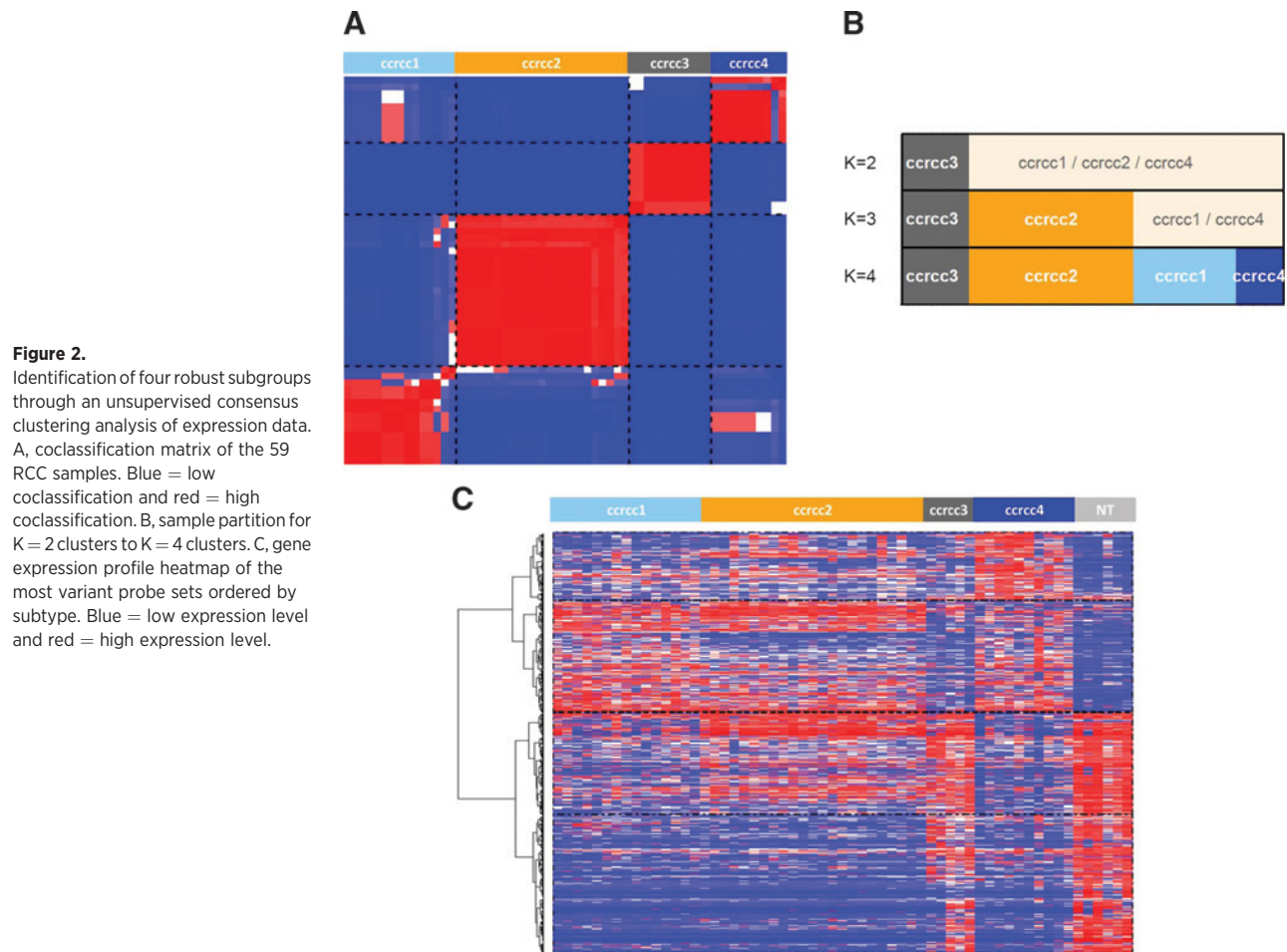


Figure 1. Clinical predictors of sunitinib response. Barplot of the clinical covariates associated with the two extreme responders: Partial or complete response (PR) versus PD. SD samples were not used for the statistical analysis. Significant ANOVA or Fisher P values: *, $P < 0.05$; **, $P < 0.01$; ***, $P < 0.001$.



IL10 as well as inhibitory receptors *LAG3* and *PD-1* (*PDCD1*) and PD-1 ligands *PD-L1* and *PD-L2* were also highly expressed (Supplementary Fig. S1). These results suggest that ccrc4 tumors display a strong inflammatory, Th1-oriented but suppressive immune microenvironment. We then assessed the expression of immune population-specific transcripts using gene signatures previously published (Supplementary Fig. S2; ref. 21). ccrc4 samples contained high amounts of B, T, and cytotoxic cells-specific transcripts, but not of natural killer cells-specific transcripts, suggesting that the cytotoxic signature in ccrc4 is mostly due to CD8⁺ T-cell infiltration. We analyzed 46 samples by immunohistochemistry and confirmed a high infiltration of CD8⁺ cells in ccrc4 tumors (Supplementary Fig. S3). Sample contamination with diploid cells was estimated to be slightly higher in ccrc4 tumors, which could reflect immune infiltration (Supplementary Fig. S5C).

Overall, 45% of the tumors were *VHL*-mutated and 32% *PBRM1*-mutated. Whereas rare mutations in *VHL* and *PBRM1* were found in ccrc4 tumors, they were frequent in ccrc1 and ccrc2 tumors but without relationship with sunitinib response (Fig. 4A and Table 2).

At a global methylation level, ccrc1/ccrc4 tumors showed more hypermethylated probes in CpG islands compared with the other subtypes (Supplementary Fig. S4A). Pathway analysis of the related hypermethylated genes showed a strong enrichment of polycomb targets (hypergeometric test,

$P < 8e-147$), and corresponding genes (*PRC2*, *SUZ12*, and *H3K27m3*) were found downexpressed (Supplementary Fig. S4B), suggesting a stem-cell phenotype for these two subtypes. The ccrc1/ccrc4 subtypes were indeed less differentiated, displaying 76% of Fuhrman grade 4 compared with 56% in ccrc2/ccrc3 tumors.

The ccrc4 subtype showed several characteristic copy-number aberrations, the most significant being 2p12, 2p22.3, and 8q21.13 amplifications (Fig. 4D; Supplementary Fig. S5; Supplementary Table S9), and both ccrc1 and ccrc4 subtypes overexpressed *MYC* targets (Fig. 4B). Amplification in the upstream region of *MYC* was found in >40% of ccrc1 and ccrc4 tumors compared with <22% in the other subtypes. Also, a CpG island was hypomethylated in the body gene of *MYC* in ccrc1/ccrc2/ccrc4 tumors as compared with ccrc3/NTs (ANOVA $P < 0.0001$), suggesting that both DNA copy number and methylation aberrations could contribute to *MYC* overexpression in the ccrc1 and ccrc4 subtypes (Supplementary Fig. S6).

Finally, the expression profile of ccrc3 samples was similar to that of NTs concerning metabolic pathways and transporter activities, consistent with the *cluster_3* described by Brannon and colleagues (ref. 5; Fig. 4B). ccrc3 tumors also showed a methylation profile similar to that of NTs (Supplementary Fig. S4C). Despite the "normal-like" characteristics of ccrc3 tumors, pathological review confirmed the tumoral nature of these samples and

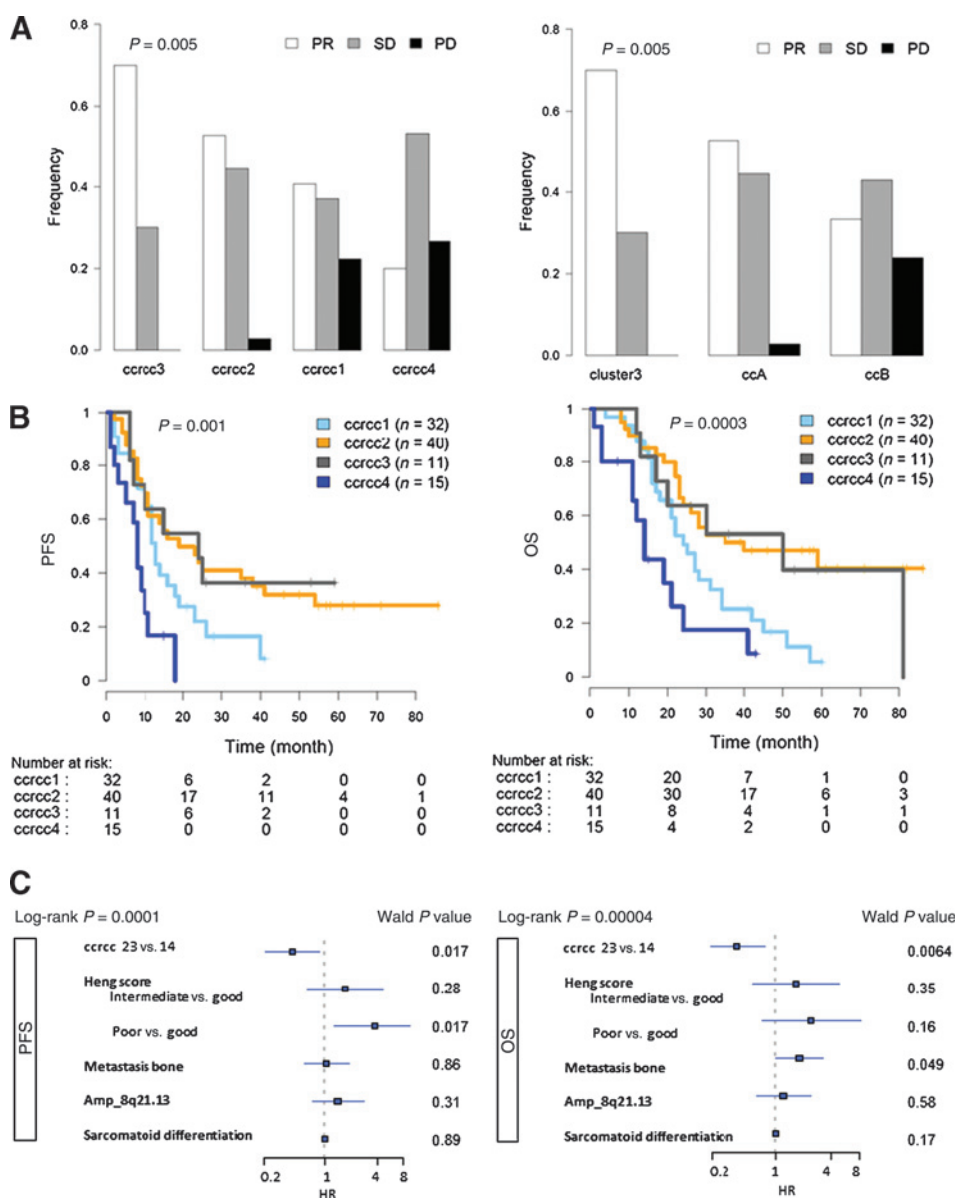


Figure 3. Correlation of the four molecular subgroups and outcome on sunitinib in the metastatic setting. A, association of sunitinib response with the unsupervised subgroups ccrcc1 to ccrcc4 (left) and the Brannon subgroups (right). The P values result from Fisher exact tests. B, association of the four unsupervised subgroups with PFS (left) and OS (right). Log-rank P values are on the top right. C, forest plots of the multivariate Cox models for PFS and OS.

their clear cell histology. The ccrcc2 subtype was not characterized by specific pathways; it always showed an intermediate expression signature, comprised between ccrcc3 and ccrcc1/ccrcc4-related profiles (Fig. 4B). ccrcc2 tumors showed the highest mutation rate for VHL. In ccrcc2 tumors, the "cellular response to hypoxia" pathway was less activated than in the ccrcc1/ccrcc4 subtypes (Fig. 4B).

Based on these molecular characteristics, we renamed our subtypes as follows: ccrcc1 = "c-myc-up," ccrcc2 = "classical," ccrcc3 = "normal-like," and ccrcc4 = "c-myc-up and immune-up" (Table 2).

Validation using the TCGA dataset

We further predicted our four subtypes in the public TCGA samples (Supplementary Fig. S7; ref. 6) with our 35-gene classifier (Supplementary Table S6). Like in our series, ccrcc3 tumors showed "normal-like" transcriptome and methylome profiles.

Somatic *PBRM1* mutations were most frequently identified in ccrcc1/ccrcc2 tumors but rarely found in ccrcc3/ccrcc4 tumors. In both series, somatic *VHL* mutations were more frequently distributed in ccrcc1/ccrcc2 tumors. The BAP1 and SETD2 mutations (data not available in our series) also showed association with the molecular subtypes: BAP1 was most mutated in the ccrcc4 tumors (P value = 0.0098) and SETD2 was most mutated in the ccrcc1 tumors (P value = 0.06). At a methylation level, in the TCGA samples, ccrcc1/ccrcc4 tumors also showed more hypermethylated probes in CpG islands compared with the other subtypes. Pathways involved in immune response and mitotic cell cycle were activated in ccrcc4 tumors, meanwhile in ccrcc3 tumors, pathways involved in hypoxia were not activated. Finally, in the TCGA cohort, 2p11.2, 8q12.1, and 8q24.3 amplifications were mostly found in ccrcc1/ccrcc4 tumors. Supplementary Fig. S8 shows the survival analysis according to our classification: ccrcc2/ccrcc3 tumors display the best survival, ccrcc1 tumors an

Table 1. Univariate Cox analyses of OS and PFS

Annotation	Value	Univariate			Multivariate		
		HR (95% CI)	P value	Log-rank P value	HR (95% CI)	P value	Log-rank P value
PFS							
Classification	ccrcc2	0.60 (0.34–1.1)	0.08	0.001			
	ccrcc3	0.56 (0.24–1.3)	0.2				
	ccrcc4	2.31 (1.1–4.7)	0.02				
Recoded classification	ccrcc1&4 vs. ccrcc2&3	0.49 (0.3–0.8)	0.004	0.004	0.42 (0.21–0.86)	0.017	0.0001
Baseline neutrophil levels	>4,500/mm ³	2.14 (1.4–3.3)	0.0004	0.0003			
Sarcomatoid dedifferentiation in tumor (%)	—	1-1.029	0.007	0.005	1.00 (0.98–1.01)	0.89	
Fuhrman grade	—	1.55 (0.99–2.4)	0.05	0.05			
ECOG-PS	—	1.54 (1.2–2)	0.001	0.001			
Amp_8q21.13	Y	1.99 (1.2–3.2)	0.004	0.003	1.41 (0.72–2.78)	0.31	
Bone metastasis	—	1.42 (0.92–2.2)	0.1	0.1	1.05 (0.58–1.90)	0.86	
IMDC (HENG) score	Intermediate	2.46 (1.1–5.4)	0.03	0.004	1.73 (0.64–4.64)	0.28	
	Poor	3.83 (1.7–8.9)	0.002		3.76 (1.26–11.22)	0.017	
MSKCC score	Intermediate	2.62 (1.2–5.8)	0.02	0.04			
	Poor	2.65 (1.1–6.2)	0.02				
OS							
Classification	ccrcc2	0.45 (0.25–0.8)	0.007	0.0003			
	ccrcc3	0.55 (0.24–1.3)	0.2				
	ccrcc4	1.93 (0.97–3.8)	0.06				
Recoded classification	ccrcc1&4 vs. ccrcc2&3	0.40 (0.24–0.66)	0.0004	0.0002	0.38 (0.19–0.76)	0.0064	0.00003
Baseline neutrophil levels	> 4,500/mm ³	1.60 (1–2.5)	0.04	0.04			
Sarcomatoid dedifferentiation in tumor (%)	—	1-1.031	0.0009	0.0005	1.01 (0.99–1.03)	0.17	
Fuhrman grade	—	1.95 (1.2–3.2)	0.008	0.007			
ECOG-PS	—	1.41 (1.1–1.8)	0.01	0.01			
Amp_8q21.13	Y	1.99 (1.2–3.2)	0.004	0.003	1.21 (0.62–2.35)	0.58	
Bone metastasis	—	1.94 (1.2–3.1)	0.004	0.003	1.81 (1.00–3.28)	0.049	
IMDC (HENG) score	Intermediate	2.67 (1.1–6.7)	0.04	0.005	1.67 (0.56–4.91)	0.35	
	Poor	4.34 (1.6–12)	0.003		2.44 (0.71–8.36)	0.16	
MSKCC score	Intermediate	3.64 (1.4–9.3)	0.007	0.02			
	Poor	3.53 (1.3–9.6)	0.01				

NOTE: Univariate models were performed on all the pathologic and clinical covariates. Only significant covariates in any of the two analyzes are indicated. Continuous variables are annotated “—” in the “value” column. For the multivariate analysis, in a first step, among all the factors that were associated with PFS and OS in univariate analysis, we excluded those factors that could be overlapping. For instance, IMDC (Heng) score and MSKCC score are redundant. We preferred IMDC (Heng) score, because the P values were more significant for PFS and OS in univariate analysis. As ECOG-PS and neutrophil count are part of the IMDC (Heng) score, they were excluded. As all tumors with sarcomatoid dedifferentiation were classified Fuhrman grade 4, we only retained sarcomatoid dedifferentiation. As a consequence, the following factors were included in the multivariate analysis, both for PFS and for OS: IMDC (Heng) score, the presence of bone metastases, the presence of sarcomatoid dedifferentiation, 8q amplification, and the classification recoded as ccrcc2+3 versus ccrcc 1+4. Abbreviation: CI, confidence interval.

intermediate survival, and ccrcc4 tumors the poorest survival ($P < 0.0001$).

Discussion

Our multi-omics analysis revealed that molecular tumor subtypes are germane to predict response, PFS, and OS, in patients with m-ccRCC treated with sunitinib. We identified 4 robust molecular subgroups of ccRCCs based on mRNA expression data. ccrcc3 (“normal-like”) and ccrcc2 tumors (“classical”) showed better sunitinib responses than ccrcc1 (“c-myc-up”) and ccrcc4 tumors (“c-myc-up and immune-up”). The ccrcc4 subtype was associated with the poorest sunitinib response. Subtype classification was the only significant covariate in multivariate analyses for PFS and OS. Survival was significantly longer for ccrcc2/ccrcc3 compared with ccrcc1/ccrcc4.

Comparison with previous ccRCC molecular classifications showed a high correlation of our four ccrcc groups with the three groups cCA, ccB, and cluster_3 described by Brannon and colleagues (4, 5; Supplementary Table S10). In particular, ccrcc3 tumors shared several characteristics of cluster_3 (5); it included all NTs

and showed a transcriptomic signature closed to normal samples (Fig. 2B and C). Although the series of Brannon and colleagues and the TCGA included both patients that were cured with nephrectomy alone as well as patients that eventually reached the metastatic setting, whereas in our series, only patients with metastatic disease were included, our subgroups are tightly related to the previously identified classification with an over-representation of the poor-prognosis ccB group, and its refinement in two subgroups, ccrcc1 and ccrcc4. Subtypes were identified using a 35-gene signature that could be useful in future tumor screening. Given the important and significant difference in RR, this classification has both predictive and prognostic potential in sunitinib-treated patients with m-ccRCC.

The incidence of *VHL* mutations was lower than the reported incidence in literature of 55% to 60% in sporadic ccRCCs. *VHL* disease-associated ccRCCs seem to grow more slowly and are associated with an overall better prognosis than sporadic ccRCCs. Sporadic ccRCCs that lack functional VHL protein might, therefore, be expected to have a better prognosis than sporadic ccRCCs resulting from *VHL*-independent mechanisms of pathogenesis. Some studies seem to support this hypothesis (26, 27), although

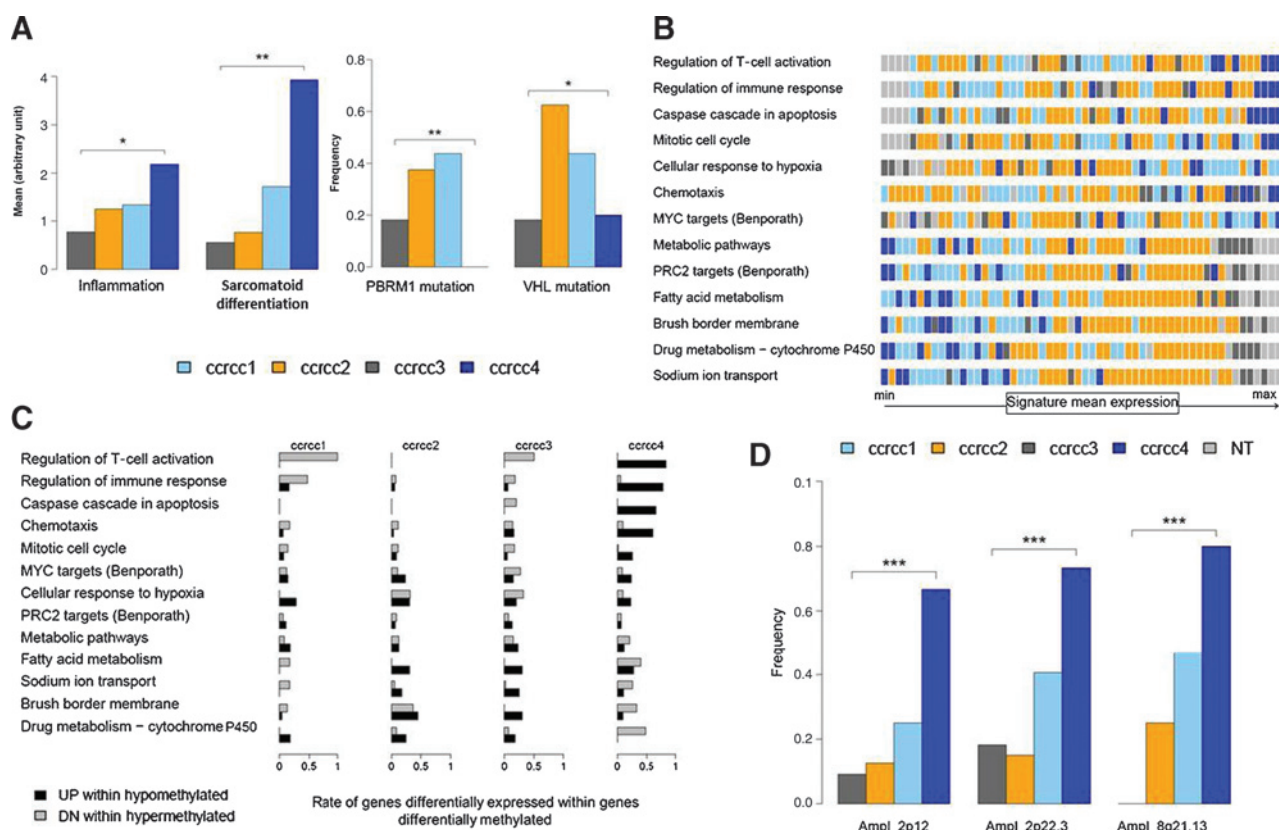


Figure 4. Clinical and molecular characteristics of the four clear cell RCC subgroups. A, barplot of the pathologic features and the incidence of *VHL* and *PBRM1* mutations associated with the four unsupervised subgroups (ccrcc1 to ccrcc4). Pathologic features were analyzed through microscopy on hematoxylin and eosin-stained slides. Tumors were screened for *VHL* and *PBRM1* mutations using direct sequencing. Significant ANOVA or Fisher *P* values: *, *P* < 0.05; **, *P* < 0.01. B, representation of the mean expression level of differentially regulated pathways between the four subgroups. Pathways are sorted by the difference between the ccrcc4 subgroup and the normal samples (NL). For a given pathway, samples are sorted by mean expression value. C, representation of the rate of upregulated genes within hypomethylated genes (black) and of the rate of downregulated genes within hypermethylated genes (gray), for each pathway. Pathways are sorted by the difference between the rates of up- and downregulated genes in the subgroup. D, barplot of the chromosomal aberrations identified by the GISTIC algorithm and associated with the ccrcc4 subtype. Significant Fisher *P* values are denoted as ***, *P* < 0.001.

others have found no association between the presence or absence of *VHL* alterations and prognosis or adverse clinical and pathologic features.

The ccrcc1/ccrcc4 subtypes, which were more closely linked with nonresponders to sunitinib, shared common molecular characteristics such as upregulation of *MYC* targets or a hypermethylated status strongly correlated with a polycomb stem-cell phenotype.

However, ccrcc4 tumors showed specific pathologic features such as a more inflammatory and sarcomatoid phenotype, an upregulation of cellular immune pathways, and an omnipresent 8q21.13 amplification. These findings are consistent with several publications showing the negative impact on outcome of an elevated baseline C-reactive protein level, a marker of inflammation, and of the presence of sarcomatoid differentiation in m-cRCC treated with anti-VEGFR TT (28–31).

Inflammation is a double-edged sword in cancer immunology. It can both fuel tumor cells growth and reinforce antitumor immunity. Consistently with our observations, extensive infiltration of CD8⁺ T cells in pulmonary metastases in patients with m-cRCC was associated with a shorter OS (22). Nonetheless, infiltrating CD8⁺ T cells are likely suppressed in this context, due

to regulatory cytokines (IL10, TGFβ1) and T-cell immunosuppressive molecules [*PD-L1* (*CD274*)] highly expressed in ccrcc4. ccRCCs are extensively infiltrated with myeloid-derived suppressor cells (32), which are likely to arise in a hypoxic environment and participate to T-cell suppression. These cells, as well as regulatory T cells, whose markers (FOXP3, IL10, and TGFβ) are also highly expressed in ccrcc4, have also been reported to allow escape from sunitinib treatment (33, 34).

Integrative analyses of the different omic experiments suggested a possible gradient of tumor progression in the following order: normal samples/ccrcc3/ccrcc2/ccrcc1/ccrcc4. We observed a metabolism switch with increasing deregulation along the ordered subtypes; similar results are obtained for the polycomb stem-cell phenotypes, the hypermethylated profile or the *MYC* target activation (Supplementary Fig. S9). These features fit the transcriptional and epigenetic sequential changes responsible for cellular reprogramming leading to acquired pluripotency by fibroblasts (35): apoptosis blockade, cell cycle activation, metabolic switch, polycomb stem-cell phenotype with the involvement of *MYC* in this cell reprogramming. Inversely, activation of the immune pathway in ccrcc4 tumors seemed more linked to a switch on/off than to a gradient. Similarly, in ccrcc4, few *VHL*/

Table 2. Summary of the molecular subtype characteristics

Subgroup (frequency)	ccrcc1 (33%)	ccrcc2 (41%)	ccrcc3 (11%)	ccrcc4 (15%)
Outcome under sunitinib				
Early PD	22.22%	2.78%	0.00%	26.67%
PR	40.74%	52.78%	70.00%	20.00%
Median OS (month)	24	35	50	14
Median PFS (month)	13	19	24	8
Clinical characteristics				
IMDC				
Good prognosis	6%	21%	18%	7%
Intermediate prognosis	69%	60%	64%	60%
Poor prognosis	25%	18%	18%	33%
MSKCC				
Good prognosis	10%	24%	27%	0%
Intermediate prognosis	58%	50%	63%	93%
Poor prognosis	32%	26%	9%	7%
Molecular characteristics				
Pathology characteristics				
Mean inflammation intensity (scale 0-3)	1.3	1.2	0.8	2.2
Mean sarcomatoid differentiation (%)	7.5	3.7	1.7	24.6
Mutations				
VHL	46.67%	62.50%	20.00%	20.00%
PBRM1	46.67%	37.50%	20.00%	0.00%
Upregulated pathways	MYC targets	Glycolysis		Immunity
	Glycolysis	Hypoxia		Apoptosis
	Hypoxia			Chemotaxis
				MYC targets
				Glycolysis
				Hypoxia
MYC expression level	++	+	-	++
Methylation status	Hypermethylated +			Hypermethylated ++
Polycomb stem-cell phenotype	++		-	+++
Copy number amplification				2p12/2p22.3/8q21.13
Proposal for names	MYC.UP	Classical	Normal like	Immun.UP/MYC.UP

PBRM1 mutations were detected, indicating that probably other gene alterations might be involved in the pathogenesis of *ccrcc4* tumors.

Hypoxia pathways are not activated in *ccrcc3* tumors and less activated in *ccrcc2* tumors than in resistant *ccrcc1/ccrcc4* tumors (Fig. 4B). Hypoxia is associated with tumor aggressiveness through higher HIF levels and expression of genes involved in tumor proliferation, vasculature, invasion, and metastatic spread leading to a poor prognosis. Through the reduction and normalization of blood vessels, anti-VEGF TT leads to better oxygen delivery in the tumor. Thus, lowering hypoxia might be an important part of the mechanism of action of anti-VEGF TT. However, tumor hypoxia was recently assessed before the start and after one month of sunitinib by a PET-CT scan with 18F-fluoromisonidazole, which accumulates in hypoxic cells. Patients with initially hypoxic targets had shorter PFS than patients with nonhypoxic targets (36). Thus, the balance of neoangiogenesis versus hypoxia could be a major trigger of response to anti-VEGF TT (37).

In a first step, as we worked on a limited number of patients, our findings should be validated in an independent patient cohort. Once validated, this molecular subtyping of tumors could probably help treatment personalization. Because patients with *ccrcc4* tumors have a short PFS under sunitinib treatment, hypomethylating agents targeting epigenetic defects (38) or immunomodulatory antibodies (39) should be preferentially tested in this subgroup of patients (40). Moreover, as even in the poor-prognosis *ccrcc4* subgroup, 20% of the patients experienced a PR, and as a placebo-treated subgroup

of patients is not available for comparison, our classification does not permit us to preclude any subgroup of patients from treatment with sunitinib. Further validation of these findings is warranted in future clinical trials integrating molecular subtyping in their design.

Disclosure of Potential Conflicts of Interest

B. Beuselinck reports receiving a commercial research grant from Pfizer. E. Becht is a consultant/advisory board member for SOTIO. S.M. Oudard is a consultant/advisory board member for Pfizer. No potential conflicts of interest were disclosed by the other authors.

Authors' Contributions

Conception and design: B. Beuselinck, A. Karadimou, A. de Reyniès, S. Oudard, J. Zucman-Rossi

Development of methodology: B. Beuselinck, N. Giraldo, S. Oudard, J. Zucman-Rossi

Acquisition of data (provided animals, acquired and managed patients, provided facilities, etc.): B. Beuselinck, A. Karadimou, V. Verkarre, G. Couchy, N. Rioux-Leclercq, V. Molinié, M. Sibony, C. Teghom, J.-J. Patard, W.H. Fridman, S. Oudard, J. Zucman-Rossi

Analysis and interpretation of data (e.g., statistical analysis, biostatistics, computational analysis): B. Beuselinck, S. Job, E. Becht, G. Couchy, V. Molinié, A. Méjean, W.H. Fridman, C. Sautès-Fridman, A. de Reyniès, S. Oudard, J. Zucman-Rossi

Writing, review, and/or revision of the manuscript: B. Beuselinck, S. Job, E. Becht, A. Karadimou, J.-J. Patard, A. Méjean, W.H. Fridman, C. Sautès-Fridman, S. Oudard, J. Zucman-Rossi

Administrative, technical, or material support (i.e., reporting or organizing data, constructing databases): B. Beuselinck, A. Karadimou, M. Sibony, J.-J. Patard, W.H. Fridman, S. Oudard, J. Zucman-Rossi

Study supervision: B. Beuselincq, R. Elaidi, A. de Reyniès, S. Oudard, J. Zucman-Rossi

Other (performed central histologic review): V. Verkarre

Acknowledgments

The authors thank sincerely for their collaboration the urologists, medical oncologists, and pathologists of the following centers, whose biologic material was used in the analysis: Angers: Centre oncologique Paul Papin: Abdel Azzouzi, Rémy Delva, Stéphane Triau, Pierre Bigot; Caen: Centre François Baclesse: Henri Bensadoun, Emmanuel Sevin, François Comoz; Créteil: Hôpital Henri Mondor: Alexandre de la Taille, Bernard Paule, Yves Allory; Suresnes: Hôpital Foch: Thierry Lebret, Christine Théodore, Yves Denoux; Leuven: University Hospitals Leuven: Hendrik Van Poppel, Evelyn Lerut, Joost Berkers, Pascal Wolter, Patrick Schöffski, Robert Paridaens; Limoges: Hôpital Dupuytren: Aurélien Descazeaud, Julien Berger, François Labrousse; Lyon: Centre Léon Bérard: Marc Colombel, Sylvie Négrier, Florence Mege-Lechevallier; Marseille: Institut Paoli-Calmettes: Franck Bladou, Gwénaëlle Gravis, Myriam Marcy; Nantes: ICO Gauducheau: Olivier Bouchot, Frédéric Rolland, Karine Renaudin; Paris: Hôpital Necker: Arnaud Méjean, Virginie Verkarre; Hôpital Cochin: Mathilde Sibony; Hôpital Tenon: Isabelle Brocheriou; Institut Mutualiste Montsouris: Pierre Validir; Clinique St-Joseph: Hervé Baumert, Gael Deplanque, Vincent Molinié; Poitiers: Jacques Irani, Jean Marc Tourani, Pierre Marie Le Villain;

Reims: Anne Durlach; Rennes: Brigitte Laguerre, Jean-Jacques Patard, Nathalie Rioux-Leclercq; Strasbourg: CHRU Strasbourg: Didier Jacqmin, Brigitte Duclos, Véronique Lindler; Tours: CHU Tours: Olivier Haillot, Claude Linassier, Franck Fetsissof. The tissue collection was coordinated by the Plateforme de Ressources Biologiques de l'Hôpital Européen Georges Pompidou in Paris. They also thank Claudia De Toma for the coordination of the tissue collection.

Grant Support

The project is funded by the PNES 2007 (Programme National d'Excellence Spécialisée) from the INCa (Institut du Cancer) and by the "Cartes d'Identité des Tumeurs" (CIT) program of the Ligue Nationale Contre le Cancer (Paris, France). B. Beuselincq received a grant from Fondation Martine Midy (Paris, France) and Fonds voor Wetenschappelijk Onderzoek Vlaanderen (Belgium). A. Karadimou received a fellowship from the Hellenic Society of Medical Oncology (Athens, Greece).

The costs of publication of this article were defrayed in part by the payment of page charges. This article must therefore be hereby marked *advertisement* in accordance with 18 U.S.C. Section 1734 solely to indicate this fact.

Received May 3, 2014; revised December 2, 2014; accepted December 6, 2014; published OnlineFirst January 12, 2015.

References

- Motzer RJ, Hutson TE, Tomczak P, Michaelson MD, Bukowski RM, Rixe O, et al. Sunitinib versus interferon alfa in metastatic renal-cell carcinoma. *N Engl J Med* 2007;356:115–24.
- Motzer RJ, Hutson TE, Tomczak P, Michaelson MD, Bukowski RM, Oudard S, et al. Overall survival and updated results for sunitinib compared with interferon alfa in patients with metastatic renal cell carcinoma. *J Clin Oncol* 2009;27:3584–90.
- Rini BI, Atkins MB. Resistance to targeted therapy in renal-cell carcinoma. *Lancet Oncol* 2009;10:992–1000.
- Brannon AR, Reddy A, Seiler M, Arreola A, Moore DT, Pruthi RS, et al. Molecular stratification of clear cell renal cell carcinoma by consensus clustering reveals distinct subtypes and survival patterns. *Genes Cancer* 2010;1:152–63.
- Brannon AR, Haake SM, Hacker KE, Pruthi RS, Wallen EM, Nielsen ME, et al. Meta-analysis of clear cell renal cell carcinoma gene expression defines a variant subgroup and identifies gender influences on tumor biology. *Eur Urol* 2012;61:258–68.
- Cancer Genome Atlas Research N. Comprehensive molecular characterization of clear cell renal cell carcinoma. *Nature* 2013;499:43–9.
- Kapur P, Pena-Llopis S, Christie A, Zhrebker L, Pavia-Jimenez A, Rathmell WK, et al. Effects on survival of BAP1 and PBRM1 mutations in sporadic clear-cell renal-cell carcinoma: a retrospective analysis with independent validation. *Lancet Oncol* 2013;14:159–67.
- Sato Y, Yoshizato T, Shiraiishi Y, Maekawa S, Okuno Y, Kamura T, et al. Integrated molecular analysis of clear-cell renal cell carcinoma. *Nat Genet* 2013;45:860–7.
- Klatte T, Kroeger N, Rampersaud EN, Birkhauser FD, Logan JE, Sonn G, et al. Gain of chromosome 8q is associated with metastases and poor survival of patients with clear cell renal cell carcinoma. *Cancer* 2012;118:5777–82.
- Monzon FA, Alvarez K, Peterson L, Truong L, Amato RJ, Hernandez-McClain J, et al. Chromosome 14q loss defines a molecular subtype of clear-cell renal cell carcinoma associated with poor prognosis. *Mod Pathol* 2011;24:1470–9.
- La Rochelle J, Klatte T, Dastane A, Rao N, Seligson D, Said J, et al. Chromosome 9p deletions identify an aggressive phenotype of clear cell renal cell carcinoma. *Cancer* 2010;116:4696–702.
- Klatte T, Rao PN, de Martino M, LaRochelle J, Shuch B, Zomorodian N, et al. Cytogenetic profile predicts prognosis of patients with clear cell renal cell carcinoma. *J Clin Oncol* 2009;27:746–53.
- Choueiri TK, Vaziri SA, Jaeger E, Elson P, Wood L, Bhalla IP, et al. von Hippel-Lindau gene status and response to vascular endothelial growth factor targeted therapy for metastatic clear cell renal cell carcinoma. *J Urol* 2008;180:860–5; discussion 5–6.
- Popova T, Manie E, Stoppa-Lyonnet D, Rigai G, Barillot E, Stern MH. Genome Alteration Print (GAP): a tool to visualize and mine complex cancer genomic profiles obtained by SNP arrays. *Genome Biol* 2009;10:R128.
- Beroukchim R, Getz G, Nghiemphu L, Barretina J, Hsueh T, Linhart D, et al. Assessing the significance of chromosomal aberrations in cancer: methodology and application to glioma. *Proc Natl Acad Sci U S A* 2007;104:20007–12.
- Boyault S, Drouet Y, Navarro C, Bachelot T, Lasset C, Treilleux I, et al. Mutational characterization of individual breast tumors: TP53 and PI3K pathway genes are frequently and distinctively mutated in different subtypes. *Breast Cancer Res Treat* 2012;132:29–39.
- Houseman EA, Christensen BC, Yeh RF, Marsit CJ, Karagas MR, Wensch M, et al. Model-based clustering of DNA methylation array data: a recursive-partitioning algorithm for high-dimensional data arising as a mixture of beta distributions. *BMC Bioinformatics* 2008;9:365.
- Monti S, Savage KJ, Kutok JL, Feuerhake F, Kurtin P, Mihm M, et al. Molecular profiling of diffuse large B-cell lymphoma identifies robust subtypes including one characterized by host inflammatory response. *Blood* 2005;105:1851–61.
- Huang Y, Niu B, Gao Y, Fu L, Li W. CD-HIT Suite: a web server for clustering and comparing biological sequences. *Bioinformatics* 2010;26:680–2.
- Tibshirani R, Walther G, Hastie T. Estimating the number of clusters in a data set via the gap statistic. *J R Stat Soc Ser B Stat Methodol* 2001;63:411–23.
- Bindea G, Mlecnik B, Tosolini M, Kirilovsky A, Waldner M, Obenauf AC, et al. Spatiotemporal dynamics of intratumoral immune cells reveal the immune landscape in human cancer. *Immunity* 2013;39:782–95.
- Remark R, Alifano M, Cremer I, Lupo A, Dieu-Nosjean MC, Riquet M, et al. Characteristics and clinical impacts of the immune environments in colorectal and renal cell carcinoma lung metastases: influence of tumor origin. *Clin Cancer Res* 2013;19:4079–91.
- Heng DY, Xie W, Regan MM, Warren MA, Golshayan AR, Sahi C, et al. Prognostic factors for overall survival in patients with metastatic renal cell carcinoma treated with vascular endothelial growth factor-targeted agents: results from a large, multicenter study. *J Clin Oncol* 2009;27:5794–9.
- Motzer RJ, Mazumdar M, Bacik J, Berg W, Amsterdam A, Ferrara J. Survival and prognostic stratification of 670 patients with advanced renal cell carcinoma. *J Clin Oncol* 1999;17:2530–40.
- Motzer RJ, Bacik J, Mazumdar M. Prognostic factors for survival of patients with stage IV renal cell carcinoma: memorial Sloan-Kettering cancer center experience. *Clin Cancer Res* 2004;10(18 Pt 2):6302S–3S.
- Yao M, Yoshida M, Kishida T, Nakaigawa N, Baba M, Kobayashi K, et al. VHL tumor suppressor gene alterations associated with good prognosis in sporadic clear-cell renal carcinoma. *J Natl Cancer Inst* 2002;94:1569–75.
- Patard JJ, Fergelot P, Karakiewicz PI, Klatte T, Trinh QD, Rioux-Leclercq N, et al. Low CAIX expression and absence of VHL gene mutation are

- associated with tumor aggressiveness and poor survival of clear cell renal cell carcinoma. *Int J Cancer* 2008;123:395–400.
28. Golshayan AR, George S, Heng DY, Elson P, Wood LS, Mekhail TM, et al. Metastatic sarcomatoid renal cell carcinoma treated with vascular endothelial growth factor-targeted therapy. *J Clin Oncol* 2009;27:235–41.
 29. Molina AM, Tickoo SK, Ishill N, Trinos MJ, Schwartz LH, Patil S, et al. Sarcomatoid-variant renal cell carcinoma: treatment outcome and survival in advanced disease. *Am J Clin Oncol* 2011;34:454–9.
 30. Fujita T, Iwamura M, Ishii D, Tabata K, Matsumoto K, Yoshida K, et al. C-reactive protein as a prognostic marker for advanced renal cell carcinoma treated with sunitinib. *Int J Urol* 2012;19:908–13.
 31. Beuselinc B, Vano YA, Oudard S, Wolter P, DeSmet R, Depoorter L, et al. Prognostic impact of baseline serum C-reactive protein in metastatic renal cell carcinoma patients treated with sunitinib. *BJU Int* 2014;114:81–9.
 32. Najjar YG, Finke JH. Clinical perspectives on targeting of myeloid derived suppressor cells in the treatment of cancer. *Front Oncol* 2013;3:49.
 33. Finke JH, Rini B, Ireland J, Rayman P, Richmond A, Golshayan A, et al. Sunitinib reverses type-1 immune suppression and decreases T-regulatory cells in renal cell carcinoma patients. *Clin Cancer Res* 2008;14:6674–82.
 34. Adotevi O, Pere H, Ravel P, Haicheur N, Badoual C, Merillon N, et al. A decrease of regulatory T cells correlates with overall survival after sunitinib-based antiangiogenic therapy in metastatic renal cancer patients. *J Immunother* 2010;33:991–8.
 35. Apostolou E, Hochedlinger K. Chromatin dynamics during cellular reprogramming. *Nature* 2013;502:462–71.
 36. Hugonnet F, Fournier L, Medioni J, Smadja C, Hindie E, Huchet V, et al. Metastatic renal cell carcinoma: relationship between initial metastasis hypoxia, change after 1 month's sunitinib, and therapeutic response: an 18F-fluoromisonidazole PET/CT study. *J Nucl Med* 2011;52:1048–55.
 37. Iacovelli R, Lanoy E, Albiges L, Escudier B. Tumour burden is an independent prognostic factor in metastatic renal cell carcinoma. *BJU Int* 2012;110:1747–53.
 38. Ricketts CJ, Morris MR, Gentle D, Shuib S, Brown M, Clarke N, et al. Methylation profiling and evaluation of demethylating therapy in renal cell carcinoma. *Clin Epigenetics* 2013;5:16.
 39. Pardoll DM. The blockade of immune checkpoints in cancer immunotherapy. *Nat Rev Cancer* 2012;12:252–64.
 40. Giraldo NA, Becht E, Remark R, Damotte D, Sautes-Fridman C, Fridman WH. The immune contexture of primary and metastatic human tumours. *Curr Opin Immunol* 2014;27C:8–15.